Experimental study of the stabilization mechanism of a lifted Diesel-type flame using combined optical diagnostics and laser-induced plasma ignition

Fabien Tagliante, Louis-Marie Malbec, Gilles Bruneaux, Lyle M Pickett, Christian Angelberger

Experimental study of the stabilization mechanism of a lifted Diesel –type flame using combined optical diagnostics and laser-induced plasma ignition

Fabien Tagliante[*a], Louis-Marie Malbec[a], Gilles Bruneaux[a], Lyle M. Pickett[b], Christian Angelberger[a]

[a] IFP Energies Nouvelles, 1 et 4 avenue de Bois-Préau – 92852 Rueil-Malmaison Cedex, (France); Institut Carnot IFPEN Transports Energies
[b] Combustion Research Facility, Sandia National Laboratories, P.O. Box 969, MS 9053, Livermore, CA 94551, USA

Abstract

The understanding of the stabilization process of Diesel spray flames is a key challenge because of its effect on pollutant emissions. In particular, the close relationship between lift-off length and soot production is now well established. However, different stabilization mechanisms have been proposed and are still under debate. The objective of this paper is to provide an experimental contribution to the investigation of these governing mechanisms. Combustion of a Diesel spray issued from a single-hole nozzle (90 µm orifice, ECN spray A injector) was studied in a constant-volume precombustion vessel using a combination of optical diagnostic techniques. Simultaneous high frame rate (6 kfps) schlieren, 355 LIF (excitation at 355 nm and maximum collection at 430 nm) and high-temperature chemiluminescence (collection from 400 nm to 490 nm) or OH* chemiluminescence (collection at 310 nm and frame rate at 60 kfps) are respectively used to follow the evolution of the gaseous jet envelope, formaldehyde location and lift-off position. Additional experiments are performed where the ignition of the mixture is forced at a location upstream of the natural lift off position by laser-induced plasma ignition (at 1064 nm). The evolution of the lift-off position until its return to the natural steady-state position is then studied for different ambient temperatures (800 K to 850 K), densities (11 kg/m3 to 14.8 kg/m3) and rail pressures (100 MPa to 150 MPa) using the same set of optical diagnostics. The analysis of the evolution of the lift off position without laser ignition reveals two main types of behaviors: sudden jumps in the upstream direction and more progressive displacement towards the downstream direction. While the former is attributed to auto-ignition events, the latter is studied through the forced laser ignition results. It is found that the location of formaldehyde greatly impacts the return velocity of the lift-off position: if laser ignition occurs upstream of the zone where formaldehyde is naturally present, the lift-off position convects rapidly until it reaches the region where formaldehyde is present and then returns more slowly towards its natural position, suggesting that cool-flame products greatly assist lift-off stabilization. The average return velocity in this second stage depends on the operating conditions.

Keywords

Lift-Off Length; high-temperature chemiluminescence; laser induced fluorescence; laser ignition; Diesel; n-Dodecane

[*] Corresponding author at: IFP Energies Nouvelles, 1 et 4 avenue de Bois-Préau – 92852 Rueil-Malmaison Cedex, (France); Institut Carnot IFPEN Transports Energies.
E-mail *address*: fabien.tagliante@ifpen.fr (Fabien Tagliante) Phone number: +33 1 47 52 60 00

1. Introduction

During the past 20 years, numerous works have allowed a better representation of combustion in direct injection Diesel engines. Especially, a conceptual model, describing the different stages of Diesel combustion has been proposed by Dec [1] and further detailed [2–4]. It describes the Diesel flame as a two-phase turbulent lifted diffusion flame with a partially premixed area upstream the base of the flame. The distance between the nozzle orifice and the flame; called the lift-off length (LOL), has been shown to play a major role in the soot formation processes [5–9]. The mechanisms explaining the stabilization of the LOL are therefore of first order in understanding and controlling soot formation in the Diesel flame, and as such, have been largely studied [9–19]. More generally, knowledge can also be gained through analogies with the stabilization processes observed in other types of lifted flames, like gaseous lifted atmospheric flames.

The stabilization mechanisms involved in this type of flames have been studied for years [20–40]. In most cases, methane has been chosen as fuel. Resulting from these studies, three main theories have been proposed to explain the flame stabilization, and are illustrated in [24]: premixed flame propagation at the flame base [25–32], flamelet quenching driven by a critical scalar dissipation rate [33,41] and stabilization due to large-scale turbulent structure [34,35].

Flame stabilization by premixed flame at the flame base approach is based on the fact that oxidizer and fuel are premixed in the lift-off area. The flame is stabilized where the mean flow velocity is equal to the turbulent flame speed. In this theory, flame stabilization occurs at the contour of the mean stoichiometric mixture [25,26]. More recently, triple flame has been proposed as one of the most convincing approaches [27–31]. A triple flame is able to stabilize even if the mean flow velocity is larger than the flame speed because the flame front is systemically located in an area where the instantaneous flow velocity has the same order of magnitude as the laminar flame speed. The triple flame is able to move to follow the stoichiometric line where the laminar flame speed is maximum [36].

The second approach, flamelet quenching, is based on small-scale turbulent structures. The lift-off occurs where the scalar dissipation rate goes under a critical value. This approach has been discussed for instance by Everest et al. [37]. They found that the local value of the scalar dissipation rate exceeds the predicted value by a factor of sixty. Schefer et al. [38] found that the value of the scalar dissipation rate was considerably below the critical value in the lift-off area. Moreover, flamelet quenching can only explain the lack of flame. Thus, it is doubtful that this theory can fully explain the stabilization mechanisms of a turbulent lifted-flame.

Thirdly, Broadwell et al. [34] have proposed a theory based on large-scale turbulent structures which carried hot combustion products to the edge of the jet. These turbulent structures can lead to upstream ignition. Otherwise, when the re-entrained products are mixed too rapidly with the unburnt jet fluid it leads to extinction. Therefore, the large-eddy structures may cause ignitions (pockets of hot burned products are transported upstream and ignite fuel/air mixture) and extinctions, as argued by Miake-Lye et al. [39], leading to flame stabilization.

Several other works have proposed hybrid stabilization mechanisms coupling the different theories mentioned previously. Burgess and Lawn [40] proposed a stabilization governed by turbulent premixed flame where the flame propagates around the periphery of the large eddies. More recently, Lawn [23] argued that large structures of rich mixture coming from the jet can move downstream and auto-ignite due to hot regions. This ignited kernel propagates downstream

with a triple flame shape leaving a ribbon of diffusion flame behind it which is drifted by the large scale.

Under Diesel conditions, the lift-off stabilization mechanisms may be different because of high-temperature, high-pressure conditions and Diesel-type fuels and two-phase flow processes. Chemical mechanisms show that Diesel fuels generally exhibits two stages of ignition chemistry [42–44]. The first stage consists of a low-temperature heat release (LTHR, often called cool flame), whereas the second stage is characterized by a high-temperature heat release (HTHR) [2]. Formaldehyde (HCHO), for the 1st stage, and OH, for the 2nd stage, are abundant and measureable species often used as markers of these stages of heat release [2,5,45] . Chemistry-turbulence interactions have been studied in order to better understand stabilization mechanisms of the flame base, and especially discriminate between the roles of the two main candidates to explain the Diesel flame stabilization: flame propagation at the flame base and auto-ignition.

Siebers and Higgins [7] and Siebers et al. [6] used an experimental correlation based on flame propagation [32] to estimate a time average LOL for Diesel flames. Comparison with experimental measurements of average LOL shows a very good agreement, suggesting that flame propagation could be the underlying stabilization mechanism. However, this time average prediction of the LOL does not take into account the nature of the fuel and it has been shown [10–13] that the LOL varied with different fuels. This lack of prediction highlights the fact that some physical phenomena have not been taken into account.

More recently, Venugopal and Abraham [46], based on Reynolds Averaged Navier-Stokes (RANS) have proposed a study of the flame stabilization under diesel conditions. In this work [46], lift-off is modeled to result from flame extinction in the near-field of the jet. The authors have carried test conditions variations in order to propose a power law estimating a time average LOL under diesel conditions. This power law has been compared to the experimental correlation [6,7]. It appears that the coefficients are in quite good agreement. However, the authors argue that it would be inappropriate to conclude that the flame extinction alone can fully explain the flame stabilization. Like highlighted for non-autoignitive conditions, flame extinction can only explain the absence of flame. Thus, other mechanisms like auto ignitions need to be taken into account to explain the flame stabilization.

Many studies have proposed auto-ignition as one of the main stabilization mechanisms [5,9,14–16]. It is clearly established that auto-ignition plays a leading role in the flame stabilization: detached auto-ignition sites upstream of the reaction zone have been observed [5,14] affecting the LOL. Pickett et al. [5] have analyzed the cool flame to investigate the auto-ignition and thus the flame stabilization through the LOL. Cool flames have been found to have a strong effect on the auto-ignition delay because it is the first stage before the high-temperature combustion. The authors [5] have argued that the location of cool flame has some bearings on the lift-off stabilization.

More recently, keeping the idea of flame propagation and auto-ignition, Krisman et al. [17,18,47,48] have proposed a stabilization mechanism including both edge-flames and auto-ignition, using dimethyl ether (DME) as fuel [17,18,47] and n-heptane [48]. As a first step based on a laminar two dimensional Direct Numerical Simulation (2D-DNS) [17]. Then this study has been enriched by a 3D-DNS of a turbulent lifted DME slot jet flame proposed by Minamoto and Chen [19] which confirms the existence of triple flames under the Diesel condition. They also have investigated the impact of the cool flame on laminar premixed flame. They found that the laminar flame speed is increased by a factor 1.3 to 1.8 compared to non-autoignitive conditions.

Recent study [49] of 1D premixed flame of DME under autoignitive conditions confirms an increase of the laminar flame speed compared to theoretical flame speed given by a power law. For example, according to [49] , the laminar flame speed computed with Cantera [50] at 1000 K is double the flame speed predicted by a power law [51]. However, it is still unclear how this rise of premixed flame velocity can impact the flame stabilization under turbulent condition.

Finally, another approach [9] is to consider that flame stabilization is due to a combination of premixed flames and large-scale turbulent structures which carry hot combustion products to the edge of the jet [34] leading to auto-ignition. This theory is built on an experimental study performing high-speed high-temperature chemiluminescence visualizations with a forced laser ignition upstream of the flame base.

To summarize, auto-ignitions have been the predominant physical phenomenon to explain the flame stabilization under Diesel condition [9–15]. However, more and more recent numerical studies have shown the presence of partially premixed flame under autoignitive conditions [16–19,52]. A review of fundamental studies relevant to flame stabilization in diesel jets proposed by Venugopal and Abraham [53] concluded that the flame stabilization can be explained by multiple theories listed above. However, mixing theories which have contradictory hypothesis demonstrates that the flame stabilization mechanisms are still not well understood. Based on the theories developed these past 50 years under gaseous lifted atmospheric flames, premixed flames under Diesel condition have been identified as edge-flame. However, it is still unclear how these edge flames can impact the flame stabilization. Therefore, the two main theories to explain the flame stabilization under Diesel condition are auto-ignitions and flame propagation. Theories coupling, auto ignitions, edge flames or turbulent large scales have also been proposed, but have never been demonstrated.

Despite the numerous studies on this topic, there is still a need of further investigations to better understand the stabilization mechanisms of lift-off for Diesel sprays. The objective of the work presented in this paper is to contribute to this understanding effort by performing an experimental investigation of the Diesel lift off stabilization process using advanced high-speed diagnostics. In particular, compared to previous experimental studies, the present work provide additional information on the effect of the low temperature chemistry on the stabilization process. Therefore, as a first step, simultaneous and time-resolved optical diagnostics are used to follow the evolution of low-temperature and high-temperature chemical activity around the lift-off length location. In a second step, using the same experimental setup than for the first step, forced laser ignitions upstream the LOL have been performed following the same methodology than [9], since the latter has proved to be a pertinent approach for providing relevant information on the stabilization process. Thus, the low- and high-temperature flame are spatially and temporally tracked after a forced ignition to investigate the stabilization mechanisms. The results are discussed to provide new information on the stabilization process of Diesel spray flames.

2. Experimental details

2.1. Experimental conditions

Experiments were conducted in an optically-accessible constant-volume combustion vessel. The vessel geometry and operation have already been extensively described in previous work [3], therefore only the main features will be recalled here. It has a cubical combustion chamber

(125 mm per side) with five optical accesses provided by sapphire windows (120 mm diameter) providing a 80 mm optical access. Pressure and temperature are increased by the combustion of a flammable mixture, and injection is triggered during the cool-down process following the combustion, when the desired temperature is reached.

A single-hole Diesel Bosch injector (90 µm orifice, ECN spray A injector [54]) is horizontally mounted on the vessel. Long injection durations (10 ms) are performed in ambient gases simulating Diesel engine thermodynamic conditions. These long injections allow for the flame to reach and stay in a steady-state regime. Specifications for the injector and ambient operating conditions are given in Table 1. The ambient oxygen percentage (volumetric) is 16 %. Variations of ambient temperature, density and injection pressure have been tested and are summarized in Table 2, where the reference case is condition α. The fuel is n-dodecane. The injection setup respects ECN recommendations.

Common rail fuel injector	Bosh solenoid-activated, generation 2.2
Injector serial #	306.22
Fuel injector nominal nozzle outlet diameter	90 µm
Nozzle K factor	K=$(d_{inlet} - d_{outet})/10[\mu m] = 1.5$
Nozzle shaping	Hydro-eroded
Mini-sac volume	0.2 mm^3
Discharge coefficient	$C_d = 0.86$
Spray full include angle	0°
Fuel	n-dodecane
Fuel temperature at nozzle	363 K (90°C)
Common rail volume/length	22 cm^3/28 cm
Distance from the injector inlet to common rail	24 cm
Fuel pressure measurement	7 cm from injector inlet

Table 1: Operating condition

Test conditions name	$\boldsymbol{\alpha}$	$\boldsymbol{\alpha'}$	$\boldsymbol{\beta}$	$\boldsymbol{\gamma}$	$\boldsymbol{\delta}$
Ambient temperature [K]	800	**850**	800	**850**	800
Ambient density [kg/m^3]	14.8	14.8	**12**	**11**	14.8
Injection pressure [MPa]	150	150	150	150	**100**
Ambient gas oxygen (by volume) [%]			16		
Effective injection duration [ms]			10		

Table 2: The different test conditions. The parameters that change compared to the reference case α are in bold characters.

2.2. Optical diagnostics and laser ignition

The experimental setup presented in Figure 1 simultaneously tracks the evolution of the gaseous jet envelope, the formaldehyde location, and the lift-off position, with and without a forced laser ignition event during injection. The characteristics of the light excitation and collection are detailed in Table 3 and are also developed in the next sub-sections.

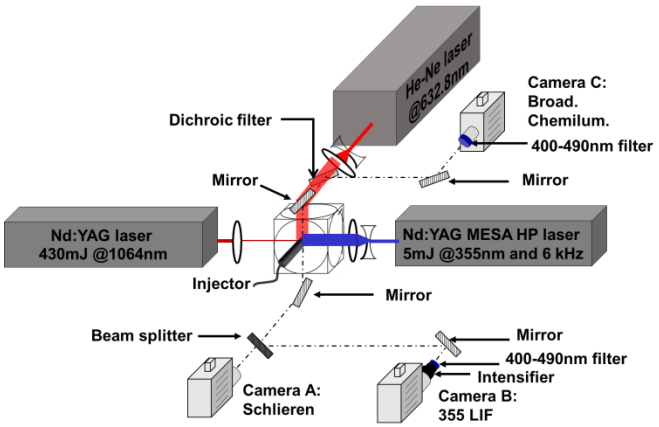

Figure 1: Experimental setup for simultaneous schlieren, 355 LIF and broadband chemiluminescence images with forced laser ignition.

355 LIF High-speed	Excitation	Continuum MESA HP Nd:YAG laser 5 mJ at 355 nm and 6kHz
	Detection	Photron SA-Z camera + intensifier at 6 kfps 445 nm filter FWHM 45 nm
355 LIF High-energy	Excitation	Quanta-Ray Nd:YAG laser 100 mJ at 355 nm (one shot)
	Detection	Photron SA-Z camera + intensifier (one frame) 445 nm filter FWHM 45 nm
Schlieren	Laser	Melles Griot He-Ne laser Continuous at 632.8 nm
	Detection	Photron SA-1 camera at 30 kfps
Broadband Chemilu.	Detection	Photron SA-Z camera at 30 kfps 445 nm filter FWHM 45 nm
OH*	Detection	Photron SA-Z camera + intensifier at 60 kfps 315 nm filter FWHM 15 nm

Table 3: Laser and imaging parameters

2.2.1. Schlieren imaging

A bright-field schlieren setup (camera A and He-Ne laser in Figure 1) was used to image the gaseous envelope of the spray. Schlieren imaging (a description of the schlieren imaging methodology is proposed in [55]) was performed using a He-Ne laser light source at 632 nm. The laser beam was expanded (×10) then diverged through a diverging lens (focal -35 mm). The laser-expanded beam covered 58 mm of the spray. The beam is next collimated with a converging lens (focal 600 mm), passed through the chamber, and then re-focused with a converging lens (focal 600 mm). A diaphragm of 0.5 mm diameter is used as spatial filter. The signal collection is performed with a high-speed Photron FASTCAM SA-1 CMOS camera equipped with a 100-mm lens. The camera was operated at a resolution of 448 × 384 pixels (58.2 × 49.9 mm), allowing for framing periods of 33.3 µs with an exposure duration of 5.6 µs. It allows sufficient temporal resolution to visualize the unsteady spray according to previous Sandia and IFPEN research [56].

2.2.2. 355 LIF

The 355 LIF technique is described in [57]. It allows the localization of formaldehyde species (HCHO), hence of low-temperature reactions occurring during the first reactions of fuel decomposition [2]. It also detects poly-aromatic hydrocarbon (PAH) molecules that are formed in high-temperature fuel-rich areas downstream of the jet [2]. But, because of different spatial locations, it is possible to discriminate between HCHO and PAH in such sprays. Here, high-speed 355 LIF is implemented in order to provide a temporal tracking of the formaldehyde cloud during Diesel injections (camera B and Nd:YAG laser in Figure 1).

High-speed 355 LIF was performed using the third harmonic of a Continuum MESA HP Nd:YAG laser generating a 355 nm pulsed beam up to 40kHz. The laser sheet measuring 35 mm long and 1 mm thick (starting at 13 mm from the injector), has been created by a collection of three lenses. The first one is a diverging lens (focal -76.2 mm), then the beam went through two converging lenses, (focal 300 mm and 500 mm) to create the final laser sheet. The signal was collected by a high-speed Photron FASTCAM SA-Z CMOS camera coupled with a Lambert Instruments HiCATT intensifier, gain set to 850. The camera was operated at a resolution of 1024 × 256 pixels (152.7 × 38.1 mm) with an 85 mm f/1.4 lens and a 455 nm filter (FWHM 45 nm). This wavelength range has been chosen to collect the spectral bands of formaldehyde in the range 410-440 nm after a 355 nm excitation [2]. A compromise has to be found between the laser repetition rate and the energy per pulse, which must be high enough to obtain enough LIF signal, which will be detailed in the Results section. To the best of our knowledge, high-speed 355 LIF has not yet been proposed in a similar configuration, thus no recommendations can be

found in the literature on the minimum energy level. Therefore, conventional single-shot LIF is proposed as the reference optical diagnostics to measure formaldehyde.

For that purpose, single-shot 355 LIF was performed using a Quanta-Ray Nd:YAG laser generating a 100 mJ laser beam at 355 nm and 10 Hz (one pulse per injection event). The same lenses combination as for the high-speed 355 LIF technique has been used, resulting in wider laser sheet (45 mm instead of 35 mm). The laser sheet starts at 8 mm and finishes at 53 mm from the injector. Because of the higher fluence of the laser, a gain of 750 (instead of 850) for the intensifier was sufficient to collect enough signal while increasing the signal/noise ratio. Only one frame per injection is acquired, 4 ms After the Start of Injection (ASI) during the quasi-steady state of the combustion. For each technique, 10 injections have been performed in order to compare ensemble-averaged images. The signals are integrated along the radial direction to obtain an average axial profile, which is then normalized by its maximum value. The results obtained with a repetition rate of 6 kHz (i.e. 5mJ per pulse) and for test condition α are presented in Figure 2. The two images on the top and in the middle are normalized by the maximum intensity of a square pixel area made of 9 pixels. The profiles are the integration of the normalized intensity along the radial axis. First of all, the spatial location of the collected signal, which is upstream of high-temperature, soot forming regions, leads to the assumption that this signal comes only from formaldehyde fluorescence and not from PAH. Indeed, previous results published in [57] for comparable ambient conditions show that it is very unlikely to collect PAH fluorescence signal for axial distances below 35 mm. Therefore, as a first step, we assumed that the acquired images are not contaminated with PAH fluorescence.

The global spatial locations of the formaldehyde clouds are similar between the two setups. However, it appears that the single-shot 355 LIF (high-energy LIF) allows a better detection of the HCHO for axial distances below approx. 25mm. To go further, the normalized average 355 LIF profiles (Figure 2 - bottom) are compared. Similar to the lift-off length defined for the high-temperature flame, a formaldehyde lift-off length LOL_{HCHO} can be computed. This is defined as the most upstream axial position where the normalized profile reaches 10% of the maximum signal. For the α test condition presented in Figure 2, it leads to a position of 22 mm for the single shot 355 LIF and 25 mm for the high-speed 355 LIF. Increasing the repetition rate of the high-speed 355 nm laser (and thus decreasing the energy per pulse) would lead to a further deterioration of the collected fluorescence signal. Test at 10 kHz and 2.2 mJ per pulses have shown a very bad signal-to-noise ratio and have been discarded. A decrease in the repetition rate would allow to increase the energy per pulse, but that would be to the detriment of temporal resolution. Therefore, a good compromise between temporal resolution and signal collected is obtained at 6 kHz and 5 mJ per pulse. However, in the following analysis, this lack of sensitivity for axial positions below 25 mm where there is low formaldehyde concentration must be kept in mind.

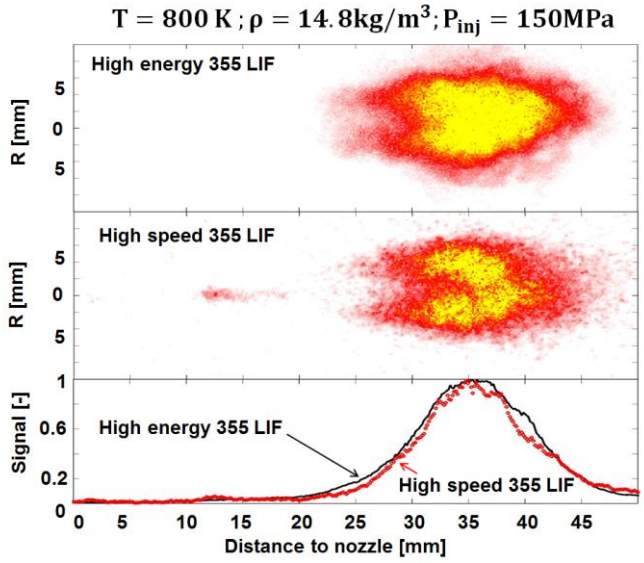

Figure 2: Average formaldehyde cloud from 355 LIF at 100 mJ (top image) and 5 mJ (middle image), normalized average 355 LIF profiles integrated radially (bottom image).

2.2.3. High-temperature chemiluminescence

Two different techniques have been used to track the high-temperature flame: OH* and broadband chemiluminescence. The former is the recommended technique, in particular within the ECN framework, because UV-range imaging minimizes contamination by soot incandescence, but it requires the use of a high-speed UV-sensitive camera (intensifier). Since only one high-speed intensifier was available for the experiments, when the latter was required for another diagnostic (high-speed 355 LIF), broadband chemiluminescence was used to determine the LOL position.

The OH* signal has been collected with a high-speed Photron FASTCAM SA-Z CMOS camera at 60 kfps coupled with a high-speed intensifier (same intensifier as for the 355 LIF). The camera was equipped with an ultraviolet transmitting lens (UV-Cerco 100-mm, f/2.8) and with a 315 nm filter (FWHM 10 nm), as recommended setup [7,8]. The resolution was 1024 × 256 pixels (117.5 × 29.3 mm) and the exposure time was 10 μs.

Broadband chemiluminescence has been collected with a high-speed FASTCAM SA-Z CMOS camera at 30 kfps, equipped with a 85mm f/1.8 lens and a 455 nm filter (FWHM 45 nm) collecting around the CH^* radical band, while rejecting the strongest emission from soot incandescence. The exposure duration was 25 μs and the resolution was 1024 × 384 pixels (113.7 × 42.6 mm).

Since broadband chemiluminescence may lack of sensitivity near the flame base and could also be polluted by soot natural incandescence signal [7,8,58], a detailed comparison of the two techniques was performed. OH* and broadband chemiluminescence have been collected simultaneously though not at the same frame-rate. Figure 3 shows a comparison between the

broadband and the OH* chemiluminescence images for 8 different timings. First, an auto-ignited kernel appears, then, this kernel merges the main flame while being convected downstream by the flow. These two techniques show good agreement, since the observed flame structures are similar. Especially, broadband chemiluminescence is able to catch the signal from the kernel appearing upstream of the flame base. However, the signal is weaker with the Broadband chemiluminescence setup, and some information can be lost in the very upstream locations of the flame. For example, at 7967 µs ASI an auto-ignited kernel appears on the OH* images whereas this kernel is not yet observed on the broadband images. However 66 µs after, the kernel is observed on both diagnostics. Therefore, high-speed OH* chemiluminescence is the preferred technique to obtain quantitative information on LOL because of its higher time and spatial resolution. A Previous study [45] performing simultaneously single-shot images of OH and formaldehyde PLIF has shown that formaldehyde is disappearing at the same position where the high-temperature flame is measured. The formaldehyde is mainly localized at the center of jet as shown in Figure 2, while OH PLIF identifies the high-temperature flame at the jet periphery. A more detailed description of the interaction between formaldehyde and the high-temperature flame is proposed in Section 3.

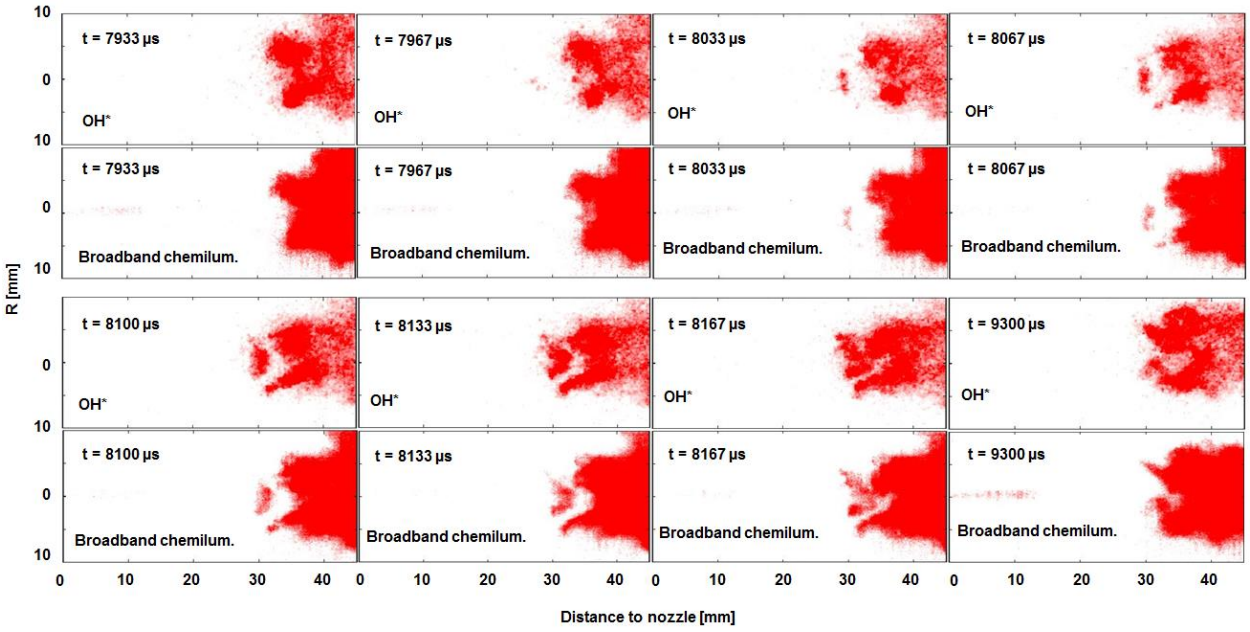

Figure 3: Instantaneous frames from OH* and broadband chemiluminescence at 30 kfps for the α test condition. The time is expressed in terms of time ASI.

2.2.4. Laser ignition

The ignition was accomplished focusing a 1064 nm beam produced by a Quanta-Ray Nd:YAG laser through a spherical 100 mm converging lens . The beam diameter before the lens

was 1 cm with an energy of 430 mJ per pulse, and a pulse duration of 8 ns. The beam diameter at the focal point has been estimated at 38 µm through equation Eq.(1) [59]:

$$d = \frac{M^2 4\lambda f}{\pi D}, \qquad (1)$$

where, d is the laser ignition beam diameter at focal point, $M^2$is the beam quality factor of the beam (M^2=2.8), λ is the laser wavelength, f is the focal length and D is the beam diameter before the focal lens. Note that Eq.(1) can only provide a rough estimation of the beam diameter because it does not take into account all the optical effects like the beam-steering. Due to the high-energy density (about 38 kJ/cm^2), plasma formation occurs [9,60], thereby igniting the air-fuel mixture. This focalization point is located on the spray axis, as confirmed by generating a plasma in pure nitrogen , as proposed in [60]. The forced laser ignitions were performed for two axial positions, the closest to the injector at 17 mm, upstream the formaldehyde cloud, and the other one at 26 mm from the injector, within the formaldehyde cloud.

3. Results and Discussion

The results are presented and analyzed with the following steps. After an analysis of the flame structure, the evolution of the low- (LOL_{HCHO}) and high- (LOL) temperature flame base locations are first analyzed without forced laser ignition, hereafter referred as "natural evolution" of the flame. Then, simultaneous observations of the gaseous jet envelope, formaldehyde location and flame position after forced laser ignition are discussed.

3.1.Flame structure

Figure 4 presents the superposition of the gas envelope of the spray (gray, schlieren), an iso-contour of the formaldehyde cloud (green, high-speed 355 LIF) and the high-temperature flame (red, broadband chemiluminescence). The two locations where the ignition laser is focused are also indicated. In the region of the formaldehyde cloud, the schlieren signal gets weaker as shown in the area pointed by the labeled arrow (a). This can be explained by the increase of the temperature caused by the cool flame that induce a decrease of the (refractive index) gradients [61,62]. Further downstream, the spray expansion and the apparition of the high-temperature flame are located in similar areas. However, the vapor envelope of the jet appears larger than the flame because hot burnt gases are present at the periphery of the flame as indicated with the labeled arrows(b). This description confirms the presence of high-temperature products localized at the jet periphery which would tend to stabilize the flame according to [9]. Therefore, Figure 4 confirms previous results [61,62] showing that the schlieren images can be used to provide a general view of the formaldehyde location and the LOL, and that burned gases exist outside the flame. In the rest of the paper, the flame stabilization mechanisms are investigated through high-temperature or OH^* chemiluminescence and 355 LIF.

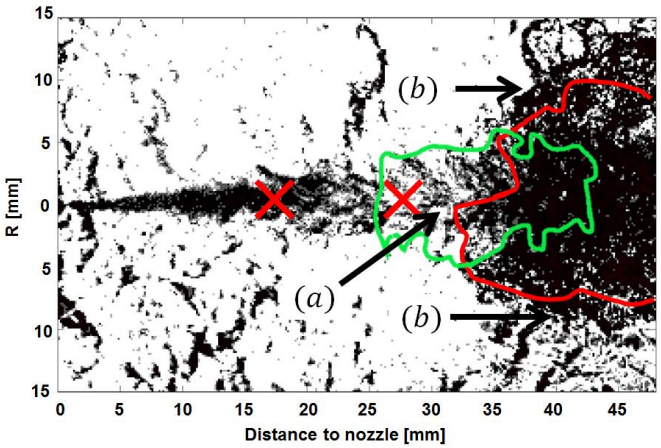

Figure 4: Superposition of an instantaneous frame from simultaneous schlieren imaging (30kfps) on an iso-contour of 355 LIF (6kfps, green line) and broadband chemiluminescence (30kfps, red line) for the α condition. The two red crosses show the location where the ignition laser is focused. (For interpretation of the references to color in this figure legend, the reader is referred to the web version of this article).

3.2. Results analysis for natural flame evolution

LOL and LOL_{HCHO} evolutions have been compared for all the test conditions without laser ignition. The results are presented in Table 4. HCHO results, obtained with both high-speed and low-speed techniques, are presented, while the high-temperature chemiluminescence results are provided through high-speed OH* chemiluminescence imaging. In the following, ensemble averages are noted <X> while time averages are noted $\bar{X}$. Time and ensemble averages are noted $<\bar{X}>$. The standard deviation of X is noted $\sigma(X)$. The High-Speed 355 LIF is indexed as follows X^{HS} while the High-Energy 355 LIF is noted X^{HE}.

Test conditions	$\boldsymbol{\alpha}$	$\boldsymbol{\beta}$	$\boldsymbol{\gamma}$	$\boldsymbol{\delta}$
$< \overline{LOL_{OH*}} >$ [mm]	35.5	49.1	44.9	31.6
$\sigma(< \overline{LOL_{OH*}} >)$ [mm]	2.5	3.5	4.3	3.1
$< LOL_{HCHO} >^{HE}$ [mm]	22.7	24.1	22.6	20.0
$\sigma(< LOL_{HCHO} >^{HE})$ [mm]	0.3	0.4	0.9	0.9
$< LOL_{HCHO} >^{HS}$ [mm]	24.5	24.0	22.7	22.7
$\sigma(< LOL_{HCHO} >^{HS})$ [mm]	0.8	0.3	0.8	1.2

Table 4: LOL and $\mathbf{LOL_{HCHO}}$ averages for the different test conditions.

$< \overline{LOL_{OH*}} >$ is the average LOL during a 1.65 ms steady period (between 1.35 and 3 ms ASI) from 10 realizations collected by high-speed OH* chemiluminescence imaging at 60 kHz. $< LOL_{HCHO} >^{HE}$ is the ensemble average of LOL_{HCHO} at high-energy. Images were acquired at 2.8 ms ASI. $< LOL_{HCHO} >^{HS}$ is the results of ensemble average formaldehyde location

$<LOL_{HCHO}>$ obtained from 10 realizations of high-speed 355 LIF. Note that none of these three diagnostics have been performed simultaneously.

As described in Section 2.2.2, the high-speed 355 LIF presents a lack of sensitivity upstream the formaldehyde cloud caused by the lower energy level of the excitation. Comparing the HE and the HS LIF, for test condition α and δ confirm this lack of sensitivity while conditions β and γ (with higher $< \overline{LOL_{OH^*}} >$) show a good agreement between the high-speed and the high-energy setup. It is not straightforward why test conditions presenting a short LOL (α and δ) present a lack of signal detection upstream the formaldehyde measured with the high-speed 355 LIF in comparison to the high energy LIF setup.

The standard deviation results of $< LOL_{HCHO} >^{HS}$ and $< LOL_{HCHO} >^{HE}$ are of the same order of magnitude, with the latter being 24% higher. It shows that the high-speed 355 LIF reasonably detects the LOL_{HCHO} fluctuations, even if not perfectly.

The standard deviation results shown for OH* and HE LIF show that on average $\sigma(< \overline{LOL_{OH^*}} >$) is 3 to 4 times greater than $\sigma(< LOL_{HCHO} >^{HE})$ hence, the upstream position of the formaldehyde cloud is much more stable than that of the high-temperature flame. In addition the fact that the standard deviations of $< LOL_{HCHO} >^{HE}$ is low shows that the average position of the formaldehyde cloud, detected with the high-energy 355 LIF, can be used to correctly define the instantaneous upstream position of the formaldehyde cloud.

Figure 5 presents LOL temporal evolutions provided by OH* chemiluminescence for two different conditions (800 K, 850 K). From a general point of view, comparing the different test conditions shows that the higher the temperature, the shorter the LOL and the weaker the absolute dispersion around the mean LOL.

More specifically, two types of characteristic evolutions are observed: event A (red rectangle) and evolution B (red line).

- Event A is characterized by very rapid upstream displacements of the LOL: in some cases, the LOL can decrease by 5 mm in less than 50 µs. These displacements are very probably caused by auto-ignitions events and will be called "large scale" auto-ignitions in the following. This evolution can be observed on Figure 3 7967 µs ASI for the α condition and also in Figure 5 (right) 5233 µs ASI for the α' condition. In both cases an isolated auto-ignited kernel appears upstream the main flame resulting in an upstream jump of the LOL.

- Evolution B is usually observed just after event A when, following a "large scale" auto-ignition event, a progressive downstream evolution is observed for a given period of time. Figure 5 (right) illustrates this downstream evolution through two images taken at 5333 and 6000 µs ASI where the LOL progressively increase. Figure 3 also shows evolution B after a "large scale" auto-ignition. Another "large scale" auto-ignition event often occurs ending phase B, significantly decreasing the LOL. The characteristic time of this evolution is approx. 0.25 ms to 1 ms.

Event A is more often observed at 800 K than at 850 K, the same remark also stands for evolution B. Indeed, the more the flame is stabilized downstream, the more auto-ignitions are

detached far from the main flame, and thus the longer evolutions B is. Interestingly, these auto-ignition sites are always located in the formaldehyde cloud for the reference case α. Figure 5 (for the α condition) shows that auto-ignitions can reduce the LOL up to 28 mm from the injector. Moreover, it has been shown in Table 4 that $< LOL_{HCHO} >^{HE}$ stays relatively stable at 22.7 mm from the injector. From all the realizations performed in this study, no auto-ignitions have been detected upstream the formaldehyde cloud. It is not possible to perform the same analysis for the α' case since no formaldehyde measurement have been performed in this cases.

The natural flame stabilization seems to be mainly governed by an alternation of event A and evolution B. The rest of the paper focuses on the analysis of the mechanisms governing the evolution B with the aim to discriminate between different potential mechanisms, in particular flame propagation, auto-ignition, or others.

Assuming a constant speed during evolution B, as illustrated by the solid lines in Figure 5, the average absolute flame front speed S_a relative to a fixed reference can be determined using Eq.(2)

$$\overline{S_a} = \frac{\Delta LOL}{\Delta t}, \qquad (2)$$

where ΔLOL and Δt are the LOL and time variation during phase B. For condition α, $\overline{S_a}$ is found equal to 6.6 m/s in average with a standard deviation of 2.8 m/s based on the eight evolutions B displayed in Figure 5. However, as can be seen on Figure 5, the apparition of phases A and B are random, which makes a systematic analysis of these phenomena on a large number of injections, or for varied ambient conditions, difficult. Forced laser ignition, whose setup is described in section 3.3, is therefore used to have reproducible and controlled apparitions of evolution B. It also allows a forcing of the ignition either in the formaldehyde cloud, or upstream of this cloud.

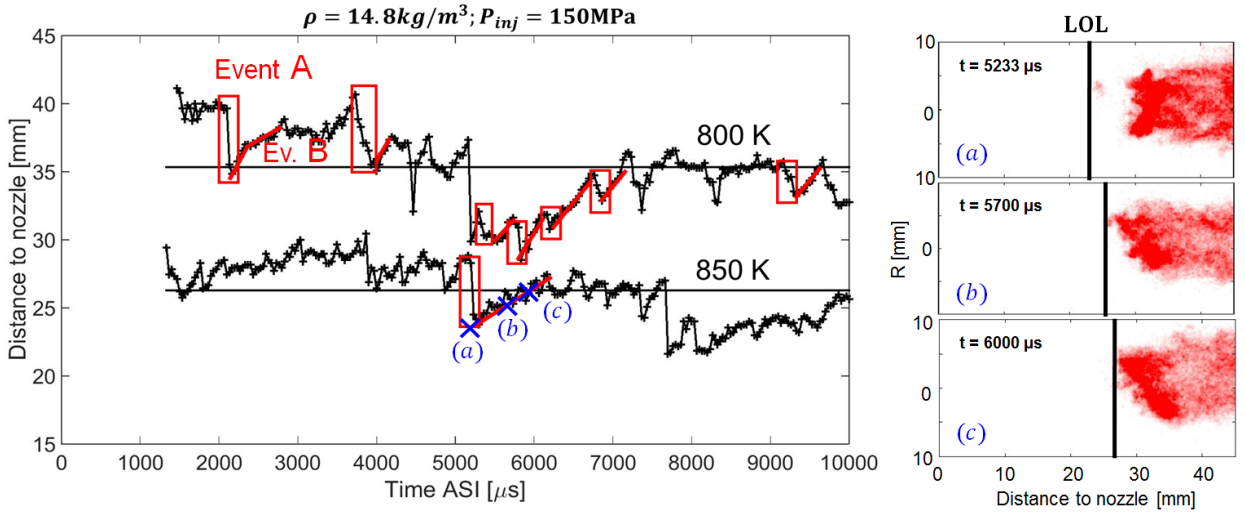

Figure 5: Left: LOL time tracking using OH* chemiluminescence imaging for ambient temperatures of 800 K and 850 K , respectively named α and α' conditions. Events A are shown as red rectangles and evolutions B as red lines for the α conditions. Right: snapshot of OH* images illustrating event A and evolution B.

3.3. Forced laser ignition

Forced laser-induced plasma ignition was used to perform a systematic analysis of phase B (downstream propagation). Indeed the advantage of laser-induced plasma ignition is that it enables to set the LOL in a location upstream of its natural position, where the conditions for natural ignition are not present and therefore where large scale auto-ignition is unlikely to occur, hence enabling to focus on the study of phase B. Laser ignition was triggered 3 ms after the effective start of injection, hence when the natural LOL is already stabilized. As detailed in the experimental setup section, two axial positions have been selected for the forced ignition as shown in Figure 4: upstream the formaldehyde cloud (17 mm downstream the orifice), and within the formaldehyde cloud (26 mm downstream the orifice).

A broadband chemiluminescence sequence at 30 kfps, showing the first 400 µs transient lift-off after a forced laser ignition is shown in Figure 6 for condition α. High-speed formaldehyde imaging is not available at such frame rate and therefore formaldehyde LIF is not shown in the Figure 6. The case shown in Figure 6 corresponds to a forced ignition at 26 mm from the nozzle orifice, hence upstream of the natural mean LOL (35 mm) but inside the formaldehyde cloud ($<LOL_{HCHO}>$ = 22 mm).

After laser ignition, the broadband chemiluminescence images present a saturation (non convected signal at the plasma location for more than 1 ms) on the top of the images. This saturation is attributed to the high plasma emission collected by the camera with a large gate width (25 µs). In comparison, OH* chemiluminescence, with a shorter gate width (10 µs), presents this saturation for less than 150 µs due to less plasma emission collected. Therefore, the saturation is ignored for the LOL detection.

The ignited kernel, created just after laser ignition, can split into two parts for analysis: the upstream part of the kernel and the downstream part. The downstream part which propagates towards the main flame in the same observation was made in [9], where it was proposed that this downwards propagation occurs in premixed flame mode. The upstream part of the kernel remains at a fixed position then after starts a slow downstream evolution. This slow downstream evolution is analyzed in more detail later in the paper using high-speed OH* chemiluminescence (60 kfps).

Interestingly, a statistical analysis, in which the radial position of the ignition location has been measured for all the test conditions, shows that although the laser beam is focused on the spray axis forced ignition occurs at a radial position between 3 and 4 mm from the jet axis. This is very probably the result of the balance between laser local fluence and local mixture ignitability. A 1D spray model [63,64] used to calculate the average mixture fraction field showed that the stoichiometric line, corresponding to a mixture fraction z_{st} = 0.048, is 2.85 mm from the centerline at this axial position. So, laser ignition occurs on the lean side of the average stoichiometric line. To further analyze this, most reactive mixture fractions have been computed with Cantera [50] using a 53-species skeletal model for n-dodecane oxidation [65] in a constant pressure reactor. The initial temperature is determined from the stoichiometric mixture fraction assuming an adiabatic mixing process. The computed most reactive mixture fractions are 0.048 at 800 K, and 0.054 for at 850 K, corresponding to a range from stoichiometric to rich mixtures. This is not consistent with the observed locations of the forced ignition, on the lean side of the average stoichiometric line. Therefore it seems that laser ignition has no requirement that it be

near a preferred self-ignition zone. The high-temperature kernels detected just after forced ignition are probably governed by plasma dynamics in a stratified mixture. Plasma breakdown begins when there is enough hydrogen, but does not mandate that this is lean or rich of stoichiometric. Once plasma forms, it becomes optically thick and absorbs the next laser radiation, which can bias the energy deposition to the lean side. Then the flame is sustained at the jet periphery for mixture near z_{st} .

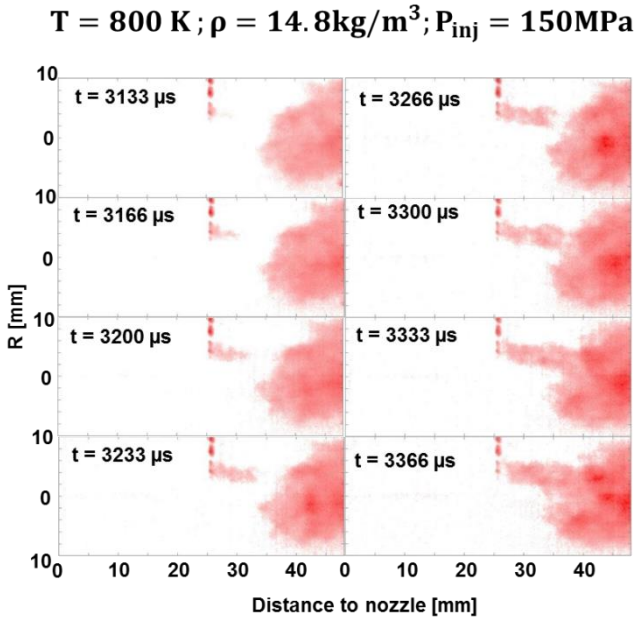

Figure 6: Broadband chemiluminescence image sequence after the laser ignition (3000 µs ASI) at 26 mm from the injector. The laser propagation is top to bottom.

Following the analysis of the very first instants after laser ignition in Figure 6, Figure 7 displays the later evolution of the flame when the ignition kernel and the main flame are already connected. Figure 7 shows a 6 kfps images sequence with simultaneous visualization of formaldehyde (green) and high-temperature flame (red). An asymmetric high-temperature flame starts at 26 mm from the injector, where the forced laser ignition occurs. The LOL increases progressively until it returns to its natural position 35mm from the orifice, as it is shown at 4366 µs ASI.

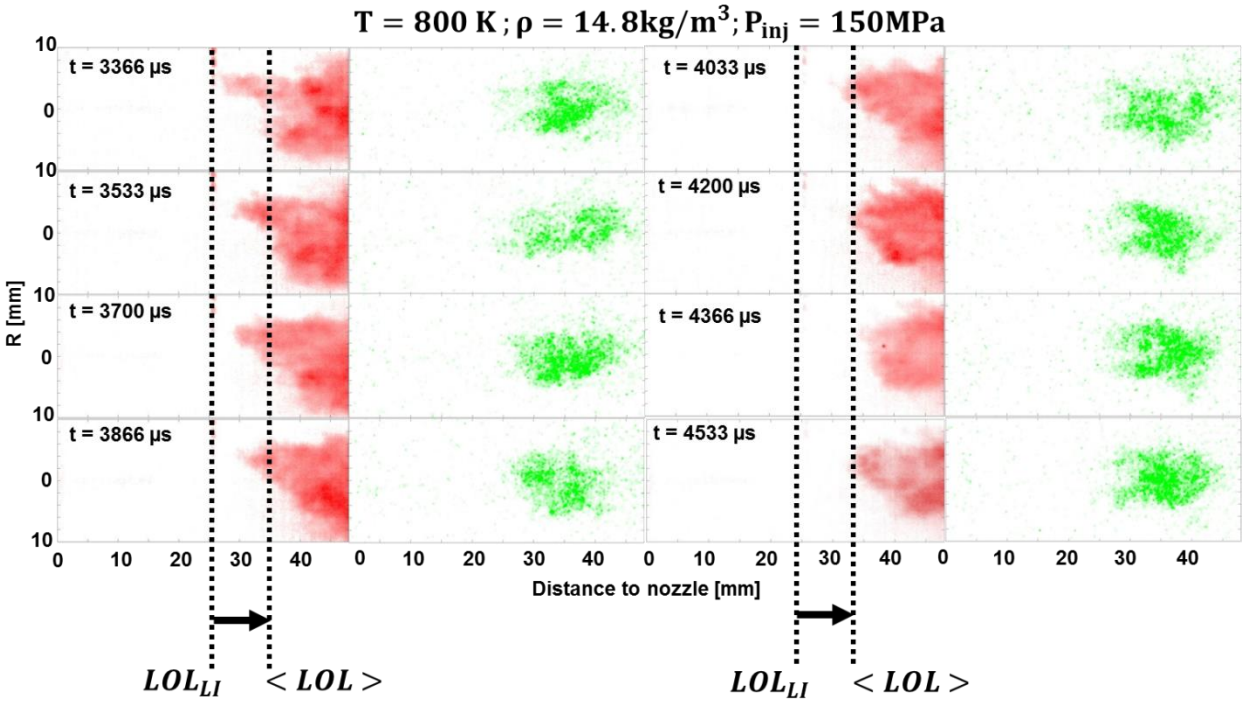

Figure 7: Broadband chemiluminescence (red, first and third columns) and 355 LIF (green, second and fourth columns) image sequence after the laser ignition (3000 µs ASI) at 26 mm from the injector, for condition α. The two dotted lines show the LOL just after the laser ignition (left line) and the average position of the "natural" LOL.

Under the limiting factor that signal to noise ratio of 355 LIF imaging is low, the formaldehyde location does not seem to be significantly affected by the ignition kernel, ignited inside the formaldehyde as shown in Figure 7. In order to further analyze the evolution of the formaldehyde cloud, Figure 8 (two top images) shows ensemble (10 realizations) and time (500 µs before and after forced ignition) averaged images provided by high-speed 355 LIF. The time is expressed in terms of time After Laser Ignition (ALI): $t_{ALI} < 0$ before the laser ignition and $t_{ALI} > 0$ after the laser ignition. In addition Figure 8 (bottom image) displays different timings of high-speed 355 LIF signal integrated along the radial direction. The left column is for laser ignition at 17 mm, upstream the formaldehyde cloud, the right column is for laser ignition at 26 mm, inside the formaldehyde cloud. The ensemble and time averaged images show a weak decrease of the LIF signal after laser ignition ($t_{ALI} > 0$), in the upper part of the formaldehyde cloud at approx. 35 mm from the injector, for both locations of laser ignition. Laser ignition also occurs in the upper part of the spray. This decrease of signal is presumably due to the formaldehyde consumption by the larger high-temperature flame generate after forced ignition like shown in Figure 7. However, 355 LIF is a planar measurement while high-temperature chemiluminescence is a line-of-sight technique. Therefore, the collected signal from broadband chemiluminescence is not necessarily located in the same plane as the formaldehyde cloud. The integrated intensity profiles shown on the bottom part of Figure 8 show that the most upstream location of the formaldehyde cloud is not affected by laser ignition. The zoomed plots shown on Figure 8 indicate that the rise of the formaldehyde signal appears at the same axial distance before and after the laser ignition, thus proving that LOL_{HCHO} is not modified by laser ignition. The small bump appearing 33µs after laser ignition (green curve on the zoomed image on the bottom left) is attributed to the plasma created by the laser.

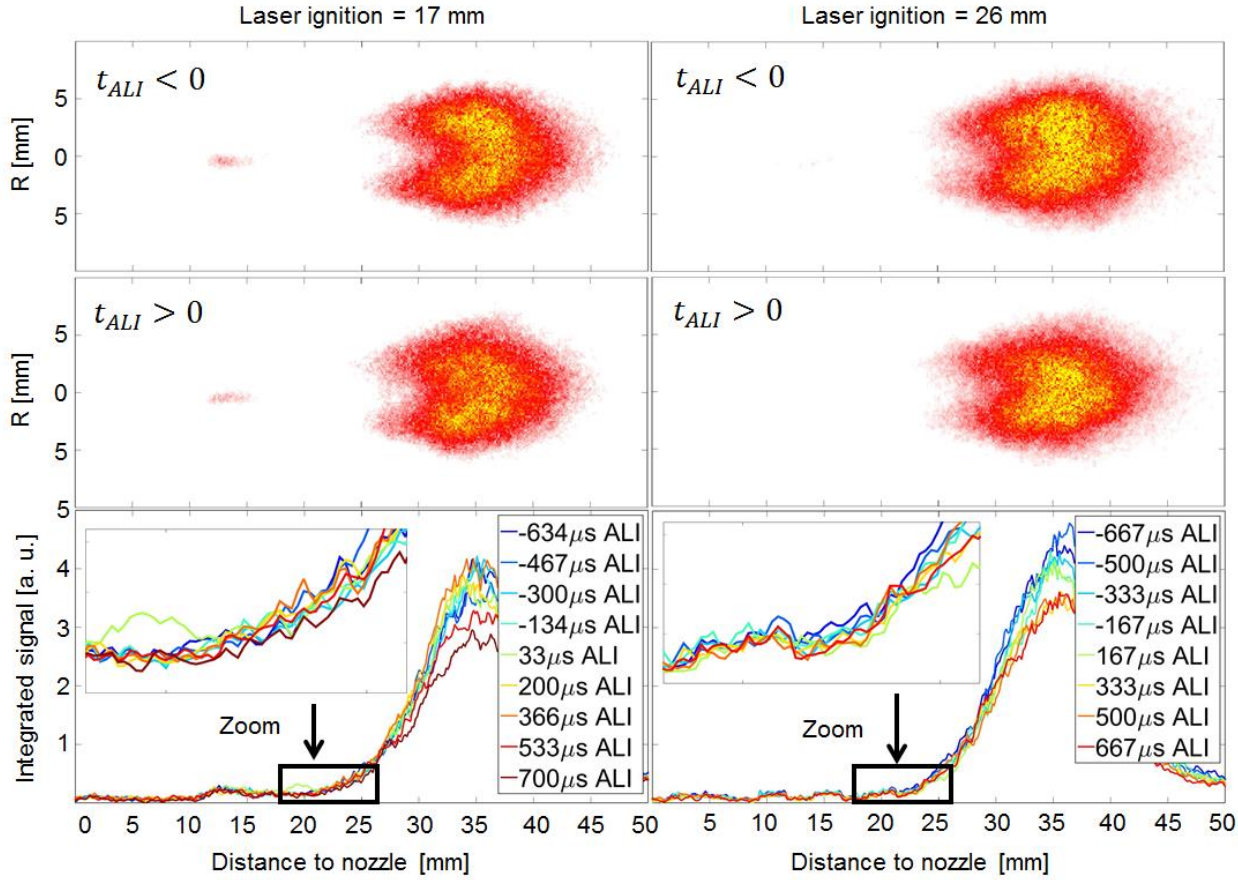

Figure 8: Ensemble and time averaged images of high-speed 355 LIF 500 µs before (first pair of images) and after (second pair of images) laser ignition. Bottom plots: ensemble averaged of high-speed 355 LIF integrated over R for different timings. (For interpretation of the references to color in this figure legend, the reader is referred to the web version of this article).

To analyze in more detail the evolution of LOL, high-speed OH* chemiluminescence measurements at 60 kfps were performed (for laser ignition upstream the formaldehyde cloud) and the corresponding evolutions are presented in Figure 9 for 16 injection events.

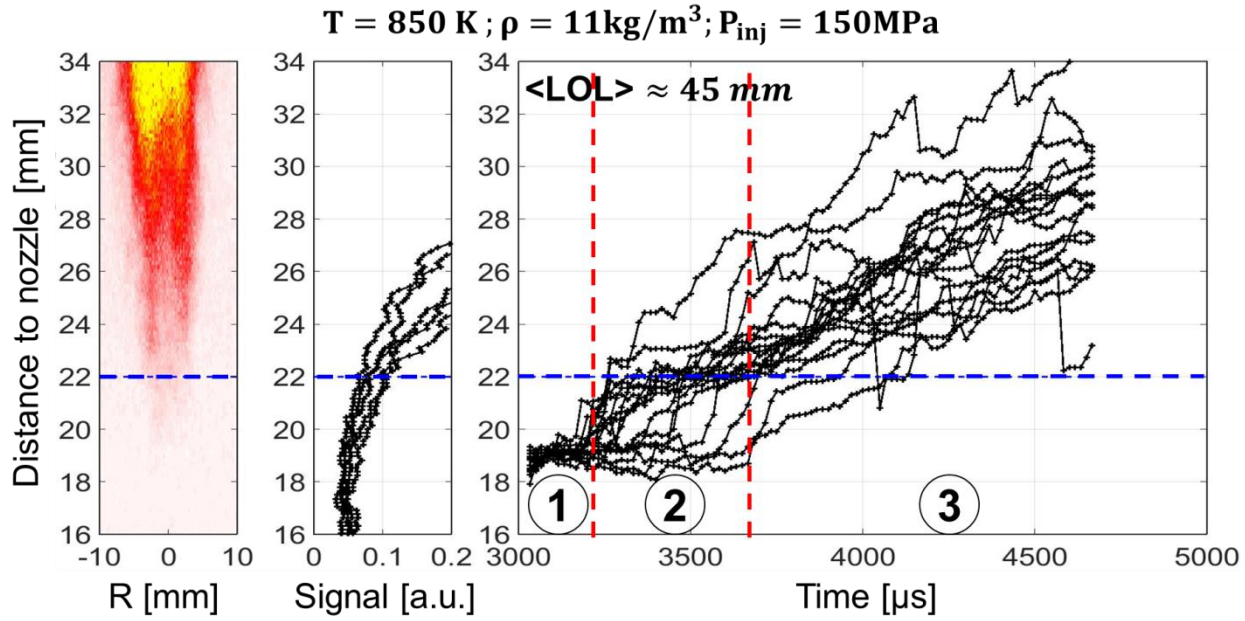

Figure 9: Averaged high-energy 355 LIF image (first column), instantaneous high-energy 355 LIF profiles integrated over R (second column), instantaneous LOL evolution after laser ignition (at 17 mm and 3000 µs) performed by OH* measurement (third column) for different injection events. The horizontal dotted blue line stands for the rising of HCHO signal at 22 mm from the injector. The two dotted vertical red lines delimit the three different stages observed after a forced laser ignition.

Figure 9 also presents an ensemble-averaged HCHO image (from high-energy 355 LIF) corresponding to 5 injections events (reported in Table 4), as well as the corresponding intensity profiles, in order to compare the LOL evolution with the formaldehyde location. Three different stages are identified.

- During the first stage, the upstream position of the ignition kernel remains fixed for 100 to 600 µs after laser ignition, near the laser ignition area. A large dispersion of the duration of this stage is observed, but it is seen systematically, and for all the test conditions.

- During the second stage, the LOL shows, in most cases, a very rapid increase up to a position around 22 mm corresponding to the value of $<LOL_{HCHO}>^{HE}$.

- The third and last stage, shows the same type of evolution as evolution B in Figure 5, with progressive increase at an almost constant speed.

The mechanisms explaining why LOL remains fixed for a given time after laser ignition (phase 1) are not straightforward. It seems that the propagation speed of the flame kernel ignited by the laser is able for some time to balance the flow velocity. Another possibility would be that the flow is affected by the laser plasma. In any case this mechanism have not been further investigated here since the authors consider that it is beyond the scope of this study. Phase 1 is very probably closely related to plasma ignition effects while the scope of the study is the evolution of the LOL after ignition, hence the following phases.

In Figure 9, the transition between stages 2 and 3 seems to be closely related to the location of formaldehyde. To confirm this observation, an analysis of the axial position corresponding to transition between stages 2 and 3 has been repeated for the other conditions and is summarized in Table 5. For laser ignition at 17 mm from the injector, the α, β and γ test conditions mostly show the 3 stages, however 40 % of the δ case exhibits only the first stage and, then, directly starts a progressive evolution without showing the second stage. Table 5 also displays an ensemble average of the transition position between the second and the third stage. Comparing these results to $< \mathrm{LOL_{HCHO}} >^{\mathrm{HE}}$ in Table 4, it appears that the turning point between the second and the last stage corresponds to the beginning of the formaldehyde cloud. Indeed, the maximum difference between $< \mathrm{LOL_{HCHO}} >^{\mathrm{HE}}$ and the transition point given in Table 5 is 5 % for the δ case. The fact that only 60 % of the realizations of the δ case shows the 3 stages is attributed to the close distance between the laser ignition and the formaldehyde cloud. Even if the laser is focused at 17 mm, due to turbulence, the ignited kernel can start growing further downstream. Additionally, regarding the standard deviation of $< \mathrm{LOL_{HCHO}} >^{\mathrm{HE}}$ (0.9 mm), for the δ condition, laser ignition inside the formaldehyde cloud can be statistically considered for this condition and thus, can explain the 40 % of realizations not showing the 3 stages. This hypothesis is confirmed by performing laser ignition within the formaldehyde cloud for the α condition. In this case, neither of the realizations show the 3 stages. When laser ignition occurs within the formaldehyde region, there is no rapid LOL increase stage, and the evolution of the LOL is more progressive, as can be observed during stage 3 (Figure 9). These results emphasize the role of the low temperature reaction region on the LOL progression speed. Upstream of the formaldehyde cloud, rapid evolutions are observed and inside the formaldehyde cloud systematic slower progression of the LOL location is observed. The mechanisms explaining the effect of the presence of formaldehyde on the LOL progression requires further analysis, but the results obtained here show that the cool flame products appear to play an important role in the LOL stabilization process.

Test conditions	$\boldsymbol{\alpha}$	$\boldsymbol{\beta}$	$\boldsymbol{\gamma}$	$\boldsymbol{\delta}$
Percentage of realizations showing the 3 stages [%]	83	72	75	60
Ensemble average of the transition position between stages 2 and 3 [mm]	22.4 (2.3)	23.1 (2.4)	22.0 (0.9)	21.0 (1.4)
Ensemble average of $\overline{S_a}$ during stage 3 [m/s]	5.0 (1.5)	7.3 (2.1)	6.5 (2.2)	3.6 (1.5)

Table 5: Statistical analysis of the three different stages identified for laser ignition at 17 mm from the injector. Standard deviations are noted in parenthesis.

The fairly linear return to the natural lift-off position (stage 3) is analyzed through Eq.(2) to determine if there are compelling observations that govern this phase for all conditions. A statistical analysis of the near-constant absolute downstream velocities ($\overline{S_a}$) measured during stage 3 for all the test conditions are summarized in last line Table 5. Table 5 is illustrated by Figure 10, where each curve was selected as being representative of the position of the transition stage 2/3 and the downstream evolution during stage 3 under the corresponding condition.

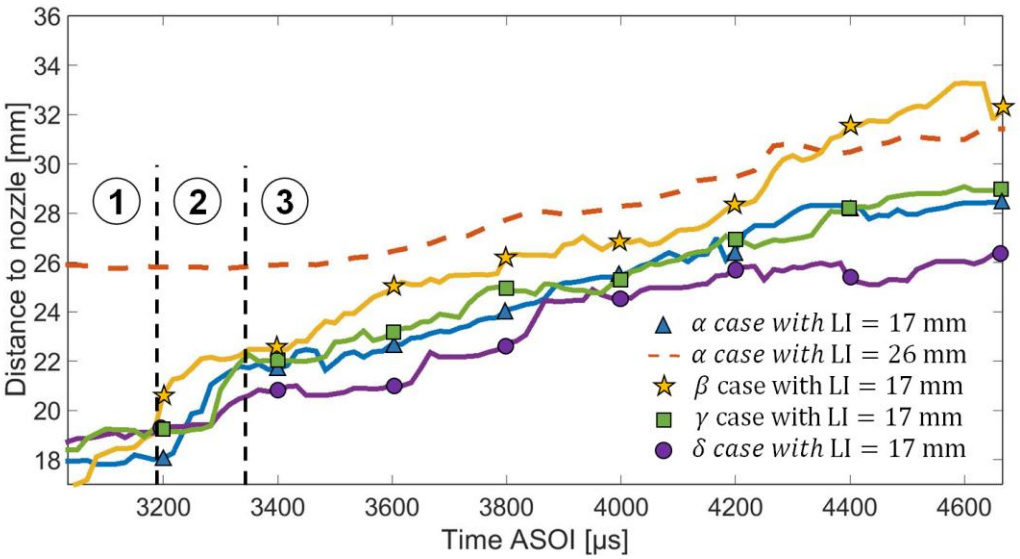

Figure 10: Instantaneous LOL tracking performed by OH* measurement (60 kfps) for the α, β, γ and δ test conditions and for laser ignition focused at 17 mm from the injector. The LOL tracking is performed by broadband chemiluminescence (30 kfps) for laser ignition at 26 mm (α test condition). When laser ignition occurs inside the formaldehyde cloud the LOL evolution are displayed with dotted lines, otherwise the LOL evolutions are plotted in solid lines.

Interestingly, $\overline{S_a}$ after forced ignition for the α condition is in the same range as $\overline{S_a}$= 6.6 m/s observed after a "natural" auto-ignition as shown on Figure 5, suggesting that the mechanisms governing the LOL evolution are similar when considering forced ignition or natural evolution. An attempt to compare the evolution of the absolute downstream velocities $\overline{S_a}$ with the flow velocity at the LOL was performed in order to investigate the role of the latter on the mechanisms governing the downstream evolution. Since no experimental velocity measurements were performed in this study, the 1D spray model [63,64] was used to provide estimations of the average velocity fields. However, no clear correlation was found between the absolute downstream velocities $,\overline{S_{a,}}$ and the average flow velocity at the LOL when taking into account the measurement uncertainties. This result shows that information on local quantities for flame structure and flow velocity are needed for such an analysis.

4. Conclusion

Combined optical diagnostics and laser-induced plasma ignition have been performed to study the stabilization mechanism of a lifted Diesel-type flame. High-temperature chemiluminescence and 355 LIF have provided the temporal evolution of the high and cool-temperature flames without and with laser ignition.

The natural LOL and LOL_{HCHO} evolutions were first analyzed. The formaldehyde cloud has been found to be much more stable than the high-temperature flame location. Auto-ignited detached kernels have always been localized inside the formaldehyde cloud and lead to a rapid decrease in the LOL while the LOL_{HCHO} remains stable. The "natural" LOL temporal evolution was analyzed for different test conditions and two typical features have been identified:

- Very rapid upstream displacement of the LOL very probably linked to auto-ignition and called "large scale" auto-ignition indicated by detached kernel upstream the main high-temperature flame
- A progressive downstream evolution of the LOL for a given period of time until another "large scale" auto-ignition occurs

The natural high-temperature flame seems to be driven by an alternation of the two above evolutions.

Forced laser ignition was performed to highlight the "natural" downstream evolution occurring after a "large scale" auto-ignition and, consequently, to investigate the main stabilization mechanism during this stage. The laser ignition was performed upstream and inside the formaldehyde cloud, demonstrating the leading role of low-temperature reaction on the downstream evolution. Upstream the formaldehyde, rapid LOL temporal evolutions are observed whereas inside the formaldehyde cloud systematic slower progression is observed.

Finally, the stabilization mechanism seems to be governed by an alternation of "large scale" auto-ignition and downstream evolution which can be governed by "small scale" auto-ignition or/and flame propagation. Moreover, the impact of the flow velocity on the possible auto-ignition fronts or/and premixed flame needs to be investigated during this downstream evolution. More investigations are needed to clarify these points and to discriminate between the propagation and auto-ignition processes.

Acknowledgments

The technical expertise of Clément Bramoullé as well as scientific discussions with Thierry Poinsot are greatly acknowledged.

References

[1] J.E. Dec, A conceptual model of DI diesel combustion based on laser-sheet imaging, SAE Technical Paper 970873 (1997).

[2] G. Bruneaux, Combustion structure of free and wall-impinging diesel jets by simultaneous laser-induced fluorescence of formaldehyde, poly-aromatic hydrocarbons, and hydroxides, Int. J. Eng. Res. 9 (3) (2008) 249–265.
[3] D. Verhoeven, J.-L. Vanhemelryck, T. Baritaud, Macroscopic and ignition characteristics of high-pressure sprays of single-component fuels, SAE Technical Paper 981069 (1998).
[4] H. Kosaka, T. Aizawa, T. Kamimoto, Two-dimensional imaging of ignition and soot formation processes in a diesel flame, Int. J. Eng. Res. 6 (2005) 21–42.
[5] L.M. Pickett, D.L. Siebers, C.A. Idicheria, Relationship between ignition processes and the lift-off length of diesel fuel jets, SAE Technical Paper 2005-01-3843 (2005).
[6] D.L. Siebers, B. Higgins, L. Pickett, Flame lift-off on direct-injection diesel fuel jets: oxygen concentration effects, SAE Technical Paper 2002-01-0890 (2002).
[7] B. Higgins, D.L. Siebers, Measurement of the flame Lift-Off location on DI diesel sprays using OH chemiluminescence, SAE Technical Paper 2001-01-0918 (2001).
[8] R. Payri, F.J. Salvador, J. Manin, A. Viera, Diesel ignition delay and lift-off length through different methodologies using a multi-hole injector, Appl. Energy 162 (2016) 541–550.
[9] L.M. Pickett, S. Kook, H. Persson, Ö. Andersson, Diesel fuel jet lift-off stabilization in the presence of laser-induced plasma ignition, Proc. Combust. Inst. 32 (2009) 2793–2800.
[10] T. Ito, T. Kitamura, M. Ueda, T. Matsumoto, J. Senda, H. Fujimoto, Effects of flame lift-off and flame temperature on soot formation in oxygenated fuel sprays, SAE Technical Paper 2003-01-0073 (2003).
[11] C. J. Mueller, W.J. Pitz, L. M. Pickett, G. C. Martin, D. L. Siebers, C. K. Westbrook, Effects of oxygenates on soot processes in DI diesel engines: experiments and numerical simulations, SAE Technical Paper 2003-01-1791 (2003).
[12] M.P.B Musculus, J.E. Dec, D.R. Tree, Effects of fuel parameters and diffusion flame lift-off on soot formation in a heavy-duty DI diesel engine, SAE Technical Paper 2002-01-0889 (2002).
[13] L.M. Pickett, D.L. Siebers, Fuel effects on soot processes of fuel jets at DI diesel conditions, SAE Technical Paper 2003-01-3080 (2003).
[14] C. Pauls, G. Grünefeld, S. Vogel, N. Peters, Combined simulation and OH-chemiluminescence measurements of the combustion process using different fuels under diesel-engine like conditions, SAE Technical Paper, 2007-01-0020 (2007).
[15] Y. Pei, E.R. Hawkes, M. Bolla, S. Kook, G.M. Goldin, Y. Yang, S.B. Pope, S. Som, An analysis of the structure of an n -dodecane spray flame using TPDF modelling, Combust. Flame 168 (2016) 420–435.
[16] C. Gong, M. Jangi, X.-S. Bai, Diesel flame lift-off stabilization in the presence of laser-ignition, Combust. Theor. Model. 19 (2015) 696–713.
[17] A. Krisman, E.R. Hawkes, M. Talei, A. Bhagatwala, J.H. Chen, Polybrachial structures in dimethyl ether edge-flames at negative temperature coefficient conditions, Proc. Combust. Inst. 35 (2015) 999–1006.
[18] A. Krisman, E.R. Hawkes, M. Talei, A. Bhagatwala, J.H. Chen, Characterisation of two-stage ignition in diesel engine-relevant thermochemical conditions using direct numerical simulation, Combust. Flame 172 (2016) 326–341.
[19] Y. Minamoto, J.H. Chen, DNS of a turbulent lifted DME jet flame, Combust. Flame 169 (2016) 38–50.
[20] K. Wohl, N.M. Kapp, C. Gazley, The stability of open flames, Symp. (Int.) Combust. 3 (1948) 3–21.
[21] K.M. Lyons, Toward an understanding of the stabilization mechanisms of lifted turbulent jet flames, Prog. Energy Combust. Sci. 33 (2007) 211–231.
[22] O. Schulz, T. Jaravel, T. Poinsot, B. Cuenot, N. Noiray, A criterion to distinguish auto-ignition and propagation applied to a lifted methane–air jet flame, Proc. Combust. Inst. 36 (2017) 1637-1644.
[23] C.J. Lawn, Lifted flames on fuel jets in co-flowing air, Prog. Energy Combust. Sci. 35 (2009) 1–30.
[24] S. Karami, E.R. Hawkes, M. Talei, J.H. Chen, Mechanisms of flame stabilisation at low lifted height in a turbulent lifted slot-jet flame, J. Fluid Mech. 777 (2015) 633–689.
[25] L. Vanquickenborne, A. Van Tiggelen, The stabilization mechanism of lifted diffusion flames, Combust. Flame 10 (1966) 59–69.
[26] H. Eickhoff, B. Lenze, W. Leuckel, Experimental investigation on the stabilization mechanism of jet diffusion flames, Symp. (Int.) Combust. 20 (1984) 311-318.
[27] H. Phillips, Flame in a buoyant methane layer, Symp. (Int.) Combust. 10 (1965) 1277–1283.
[28] L. Muñiz, M.G. Mungal, Instantaneous flame-stabilization velocities in lifted-jet diffusion flames, Combust. Flame 111 (1997) 16–31.
[29] P.N. Kioni, B. Rogg, K. Bray, A. Liñán, Flame spread in laminar mixing layers, Combust. Flame 95 (1993) 276–290.
[30] P. Domingo, L. Vervisch, Triple flames and partially premixed combustion in autoignition of non-premixed turbulent mixtures, Symp. (Int.) Combust. 26 (1996) 233–240.
[31] G.R. Ruetsch, L. Vervisch, A. Liñán, Effects of heat release on triple flames, Phys. Fluids 7 (1995) 1447–1454.

[32] N. Peters, Turbulent Combustion, Cambridge University Press, 2000.
[33] N. Peters, Laminar diffusion flamelet models in non-premixed turbulent combustion, Prog. Energy Combust. Sci. 10 (1984) 319–339.
[34] J.E. Broadwell, W.J. Dahm, M.G. Mungal, Blowout of turbulent diffusion flames, Symp. (Int.) Combust. 20 (1985) 303–310.
[35] W.M. Pitts, Assessment of theories for the behavior and blowout of lifted turbulent jet diffusion flames, Symp. (Int.) Combust. 22 (1989) 809–816.
[36] T. Poinsot and D. Veynante, Theoretical and Numerical Combustion, Third Edition, 2005.
[37] D.A. Everest, D.A. Feikema, J.F. Driscoll, Images of the strained flammable layer used to study the liftoff of turbulent jet flames, Symp. (Int.) Combust. 26 (1996) 129–136.
[38] R.W. Schefer, M. Namazian, E. Filtopoulos, J. Kelly, Temporal evolution of turbulence/chemistry interactions in lifted, turbulent-jet flames, Symp. (Int.) Combust. 25 (1994) 1223–1231.
[39] R.C. Miake-Lye, J.A. Hammer, Lifted turbulent jet flames, Symp. (Int.) Combust. 22 (1989) 817–824.
[40] C.P. Burgess, C.J. Lawn, The premixture model of turbulent burning to describe lifted jet flames, Combust. Flame 119 (1999) 95–108.
[41] N. Peters, F.A. Williams, Liftoff characteristics of turbulent jet diffusion flames, AIAA J. 21 (1983) 423–429.
[42] C.K. Westbrook, W.J. Pitz, O. Herbinet, H.J. Curran, E.J. Silke, A comprehensive detailed chemical kinetic reaction mechanism for combustion of n-alkane hydrocarbons from n-octane to n-hexadecane, Combust. Flame 156 (2009) 181–199.
[43] Z. Luo, S. Som, S.M. Sarathy, M. Plomer, W.J. Pitz, D.E. Longman, T. Lu, Development and validation of an n-dodecane skeletal mechanism for spray combustion applications, Combust. Theor. Model. 18 (2014) 187–203.
[44] R.N. Dahms, G.A. Paczko, S.A. Skeen, L.M. Pickett, Understanding the ignition mechanism of high-pressure spray flames, Proc. Combust. Inst. 36 (2017) 2615–2623.
[45] N. Maes, M. Meijer, N. Dam, B. Somers, H. Baya Toda, G. Bruneaux, S.A. Skeen, L.M. Pickett, J. Manin, Characterization of Spray A flame structure for parametric variations in ECN constant-volume vessels using chemiluminescence and laser-induced fluorescence, Combust. Flame 174 (2016) 138–151.
[46] R. Venugopal and J. Abraham, A numerical investigation of flame lift-off in diesel Jets, Combust. Sci. Technol. 179 (2007) 2599–2618.
[47] A. Krisman, E.R. Hawkes, M. Talei, A. Bhagatwala, J.H. Chen, A direct numerical simulation of cool-flame affected auto-ignition in diesel engine-relevant conditions, Proc. Combust. Inst. 36 (2017) 3567–3575.
[48] A. Krisman, E.R. Hawkes, J.H. Chen, Two-stage auto-ignition and edge flames in a high pressure turbulent jet, J. Fluid Mech. 824 (2017) 5–41.
[49] A. Krisman, E.R. Hawkes, J.H. Chen, The structure and propagation of laminar flames under autoignitive conditions, Combust. Flame 188 (2018) 399–411.
[50] D. G. Goodwin, H. K. Moffat, R. L. Speth, 2015, URL: http://www.cantera.org .
[51] M.C. Krejci, O. Mathieu, A.J. Vissotski, S. Ravi, T.G. Sikes, E.L. Petersen, A. Kérmonès, W. Metcalfe, H.J. Curran, Laminar Flame Speed and Ignition Delay Time Data for the Kinetic Modeling of Hydrogen and Syngas Fuel Blends, J. Eng. Gas Turbines Power 135 (2013) 21503.
[52] S. Deng, P. Zhao, M.E. Mueller, C.K. Law, Stabilization of laminar non-premixed DME/air coflow flames at elevated temperatures and pressures, Combust. Flame 162 (2015) 4471–4478.
[53] R. Venugopal, J. Abraham, A Review of Fundamental Studies Relevant to Flame Lift-off in Diesel Jets, SAE Technical Paper 2007-01-0134 (2007).
[54] L. M. Pickett, available at http://www.sandia.gov/ecn/ 2015.
[55] Panigrahi and Muralidhar Schlieren and Shadowgraph Methods in Heat and Mass Transfer (2012).
[56] L.M. Pickett, C.L. Genzale, G. Bruneaux, L.-M. Malbec, L. Hermant, C. Christiansen, J. Schramm, Comparison of diesel spray combustion in different high-temperature, high-pressure facilities, SAE Int. J. Engines 3 (2010) 156–181.
[57] J.M. García-Oliver, L.-M. Malbec, H.B. Toda, G. Bruneaux, A study on the interaction between local flow and flame structure for mixing-controlled diesel sprays, Combust. Flame 179 (2017) 157–171.
[58] D.L. Siebers, B. Higgins, Flame Lift-Off on Direct-Injection Diesel Sprays Under Quiescent Conditions, SAE Technical Paper 2001-01-0530 (2001).
[59] Idex optics & photonics, Gaussian beam optics, https://www.cvilaseroptics.com/file/general/All_About_Gaussian_Beam_OpticsWEB.pdf.
[60] C.L. Genzale, L.M. Pickett, A.A. Hoops, J.M. Headrick, Laser ignition of multi-injection gasoline sprays, SAE Technical Paper 2011-01-0659 (2011).
[61] P.M. Lillo, L.M. Pickett, H. Persson, O. Andersson, S. Kook, Diesel spray ignition detection and spatial/temporal correction, SAE Int. J. Engines 5 (2012) 1330–1346.

[62] S.A. Skeen, J. Manin, L.M. Pickett, Simultaneous formaldehyde PLIF and high-speed schlieren imaging for ignition visualization in high-pressure spray flames, Proc. Combust. Inst. 35 (2015) 3167–3174.
[63] J. Naber, D.L. Siebers, Effects of gas density and vaporization on penetration and dispersion of diesel sprays, SAE Technical Paper 960034 (1996).
[64] M.P.B Musculus, K. Kattke, Entrainment waves in diesel jets, SAE Int. J. Engines 2 (2009) 1170–1193.
[65] T. Yao, Y. Pei, B.-J. Zhong, S. Som, T. Lu, K.H. Luo, A compact skeletal mechanism for n -dodecane with optimized semi-global low-temperature chemistry for diesel engine simulations, Fuel 191 (2017) 339–349.